Power Loss and Performance Analysis of a Permanent Magnet Synchronous Motor for Actuator Applications

Ahmed Tameemi, Michele Degano, Mauro Di Nardo, Mukhammed Murataliyev, David Gerada, Zeyuan Xu and Chris Gerada

***Abstract* -- Permanent magnet synchronous motors are very suitable in applications demanding high power density with high performance requirements, such as in aerospace actuators. Achieving high performance targets while keeping the total weight of the electrical machine to minimum values is quite challenging and requires an ideal machine design with a comprehensive understanding of power losses. As a result, this paper focuses on a detailed investigation of losses and machine performance, taking into account different operating conditions. Furthermore, 3D FE models were used in this work to accurately predict eddy current losses in the rotor components. Finally, the experimental findings obtained from the prototype are provided to highlight the efficiency of the developed numerical models and to verify the machine design. The analysis results are in good agreement with the experimental results with a maximum 3.2% error in terms of efficiency.**

***Index Terms*--Finite element method (FEM), PMSM, Performance analysis, Power loss.**

I. Introduction

WITH ongoing advances in the aviation sector, most of the traditional hydraulic actuation systems are being partially or completely replaced by electrically actuated systems [1, 2]. The major advantage is that this removes need for complicated mechanical pipelines, reducing total weight and oil leakage while increasing efficiency [3]. Modern aircraft actuation systems are classified into Electro Hydraulic Actuators (EHAs) and Electro Mechanical Actuators (EMAs), in which the electric motor is the primary element and plays a key role in the overall performance of the actuation system [4, 5].

Today, the majority of aerospace actuation systems comprise brushless permanent magnet (BLPM) motors [6, 7]. Permanent Magnet Synchronous Machine (PMSM) is a type of brushless PM machine. They are recognized for their highly outstanding torque and power density characteristics, low power losses, high efficiency and design flexibility [8]. However, the primary drawbacks of these machines are linked to the expensive cost of the PMs as well as their intrinsic sensitivity to demagnetization and temperature [9].

The challenges for the design of high power density and high speed machines lie in the combination of the large electrical loading needed by an often restricted envelope size with the inertia-constrained rotor size. The large electrical loading might result in a significant amount of copper losses in the form of heat. While high running speeds cause a considerable rise in machine iron losses, ac losses (i.e. eddy current losses) are often more prevalent in stator windings and rotor [10]. Furthermore, high speeds increase friction losses in the bearings and windage losses within the airgap significantly [11]. For this reason, a comprehensive knowledge of power losses and their impact on machine performance is mandatory to develop an electrical machine with a higher speed, higher power density and faster dynamic response. This knowledge may then be transferred into design processes, allowing the machine designer to enhance the machine's thermal and magnetic limits, and therefore of the entire system [12].

In this paper a machine prototype is built and tested to validate all of the above. The performance of the PMSM and developed finite element (FE) models is highlighted through a comparison of numerical and experimental findings for various operating points.

II. Designed PMSM and Its Specifications

Following a comprehensive analysis combined with a detailed design that included electromagnetic, thermal, and mechanical aspects, an 8-pole, 9-slot PMSM was developed for the actuator application [13, 14]. Although the 8 poles/9 slots combination has an inherent unbalanced magnetic pull (UMP), its exceptionally low torque ripple and high efficiency make it an acceptable option for the required application [13, 14]. Table 1 summarizes the most critical characteristics of the designed machine at two distinct operating points while Fig. 1 depicts the designed machine's schematic view.

TABLE I
Key Characteristics of PMSM

Parameters	**10.5 Nm @ 8700rpm**	**5 Nm @ 19000 rpm**
DC link voltage (V)	270	
Rated current (A)	85	
Split ratio	0.535	
Airgap length (mm)	0.9	
Current density J (A/mm^2)	27.2	
Efficiency (%)	91.2	86.5
Torque ripple (%)	0.5	0.8
Moment of inertia ($kg \cdot m^2$)	$1.e^{-4}$	

Ahmed Tameemi is with Al-Farahidi University, Department of Communication Technical Engineering, Baghdad, Iraq (e-mail: Ahmed.altimimy@uoalfarahidi.edu.iq).

Ahmed Tameemi, Michele Degano, Mauro Di Nardo, Mukhammed Murataliyev, David Gerada, Zeyuan Xu and Chris Gerada are with the Power Electronics, Machines and Control (PEMC) Research Group, University of Nottingham, Nottingham, NG7 2GT, U.K.

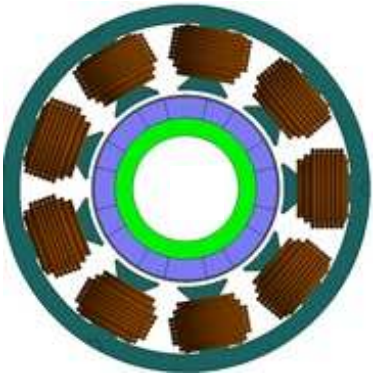

Fig. 1. Cross-section of 8p/9s PMSM

III. Power Loss Analysis

A. Copper Losses

To enhance thermal estimation, it is necessary to incorporate the AC losses impact into the copper losses prediction to guarantee that they do not significantly affect the temperatures. Indeed, the machine's high fundamental frequency of 1266.67 Hz required the use of stranded wire to mitigate AC copper losses due to the skin and proximity effects. Fig. 2 illustrates a cross-section of the designed machine's slot winding with various numbers of parallel strands but the same number of turns per coil (12 turns) and phase current (80 A) to study the influence of parallel strands on minimizing AC losses. Furthermore, to ensure the accurate distribution of eddy currents, particularly at high frequencies, a refined mesh has been established for the slot area. Finally, the impact of armature reaction and PM rotor flux on proximity losses has been taken into account.

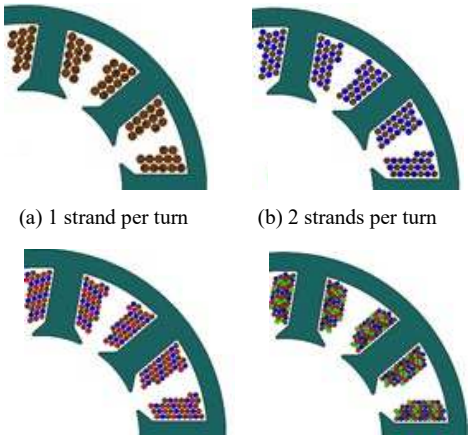

(a) 1 strand per turn (b) 2 strands per turn

(c) 3 strands per turn (d) 4 strands per turn

Fig. 2. Cross-section of stator core with.

Fig. 3 presents the ratio of copper losses (AC+DC)/DC as a function of machine running frequency. It is apparent that the overall copper losses at maximum speed are approximately 26% more than DC losses when only 1 strand per turn is used. Therefore, copper losses will be greatly underestimated if proximity and skin losses are not included. In contrast, as the number of strands increases, copper losses decrease and the rate of improvements decreases progressively. Indeed, when the number of strands is 4, variations in copper losses (AC+DC)/DC are small. As a result, 4 strands per turn were chosen.

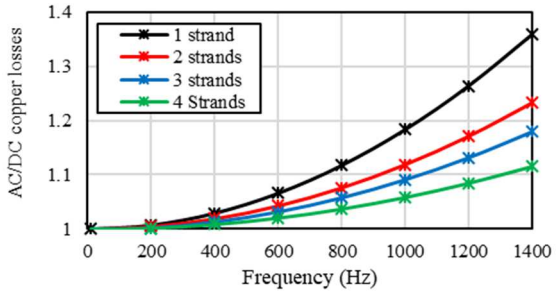

Fig. 3. Ratio of copper losses (AC+DC/DC) for various strand numbers.

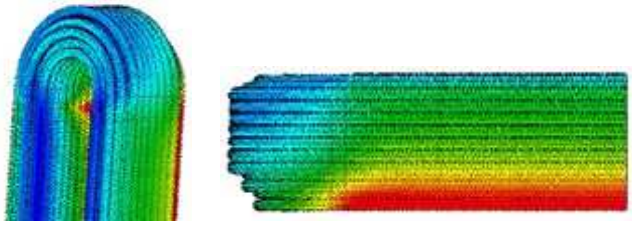

(a) Top to bottom view (b) Side view

Fig. 4. Flux density distribution in the stator winding using 3D FE model.

Fig. 4 depicts the stator conductor's magnetic flux density distribution. When compared to the slot top region, the leakage flux is greater in the slot opening region, resulting in significant eddy currents being induced near to the slot opening. As a result, it is favorable to arrange the conductors away from the slot opening area and towards the top of the slot to minimize ac losses caused by leakage flux, which leads to a non-uniform current density distribution within conductors.

B. Stator Core Losses

In high-speed electrical machines, iron loss accounts for a significant portion of overall power losses. Fig. 5 shows the stator core losses of the 8p/9s PMSM at various operating speeds. Clearly, for no load, core losses increase with speed, Fig. 5 (a). This is mostly because the magnetic flux in the stator core is linked to the permanent magnet only and remains almost constant as the frequency increases, resulting in increased iron losses. Moreover, the iron losses increase at full load condition due to both the frequency and flux density of the permanent magnet and armature reaction, particularly from 0 to 9000 rpm. While at speeds ranging from 9000 to 19000 rpm, the total iron losses decrease until specific frequencies, at which point it begins to rise despite an increase in electric frequency. This is due to the application of a field weakening process to drive the machine to higher speed, which results in a decrease in the flux density of the stator core. Additionally, the core losses caused by the end-effects (3D-effects) are investigated. The end-winding leakage flux increases the flux density near the border of tooth-shoe, thereby further contributing to core losses. Fig. 5 (b) illustrates the PM machine stator core losses for various q-axis currents at 8700 rpm (rated speed). Core losses calculated using 3D-FEA are lower than those estimated using 2D-FEA for low current values, i.e. less than 65 A, due to the leakage effect, which leads to a reduced magnet flux density in the machine's core. In contrast, the core losses anticipated by 3D-FEA are higher than those predicted by 2D-FEA at higher current levels, i.e. above 65 A, mainly because of the flux produced by the end-windings, which generates extra losses.

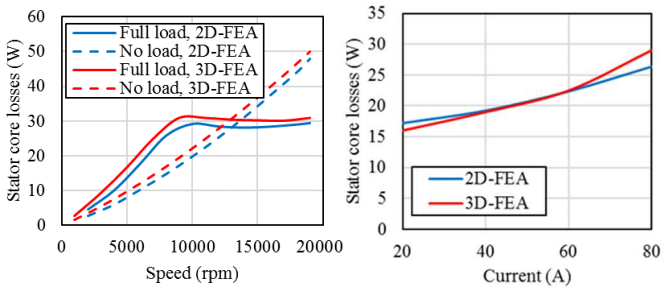

(a) Different speeds (b) Different q-axis currents

Fig. 5. Stator core losses at.

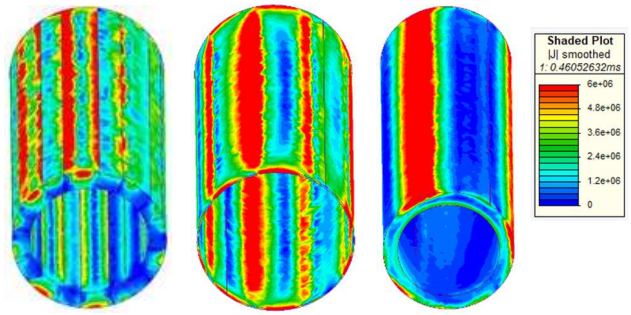

(a) Magnet (a) Sleeve (c) Shaft

Fig. 6. Eddy current density distribution for different rotor parts.

C. *Rotor Eddy-Current Losses*

Eddy current losses can also be induced in the rotor components due to the high conductivity of the sleeve, PMs, and the stainless-steel shaft. The major source of rotor losses are the stator slotting effect and space harmonics caused by winding distribution [15]. With concentrated winding, losses are particularly significant for fractional slot PMSM, as the armature field has high harmonics [16]. The corresponding distributions of eddy current density in the motor rotor at maximum speed of 19000 rpm are shown in Fig. 6. While the results for various speeds and q-axis currents are also shown Fig. 7. It is obvious that the effects of the no-load eddy current losses resulting from the stator slot are not significant as the machine is designed with a semi-open slot. In full load conditions, however, magnet losses increase substantially with speed, owing mostly to the effects of armature reaction harmonics and frequency as illustrated in Fig. 7 (a). While, 3D-FEA resulted in lower eddy current losses than 2D-FEA at the same operating point in Fig. 7 (b). This is due to the reduced leakage flux in 2D-FEA, since it does not represent end-flux leakage effects but instead constrains the flux lines.

To enhance the efficiency of the motor, eddy current losses, which are a major concern, are minimized in permanent magnets by the use of PM segmentation. 3D FE simulations are used to investigate the performance of the 8p/9s PMSM with axially segmented magnets. Fig. 8 illustrates the magnet's axial segmentation impact on eddy current losses at two different operating speeds. As illustrated in Fig. 8 (a), increasing the number of magnet segments results in a progressive reduction in magnet eddy current loss. However, doubling the number of magnet segments might lead to a 20% rise in cost per rotor, as well as making the assembly process more difficult.

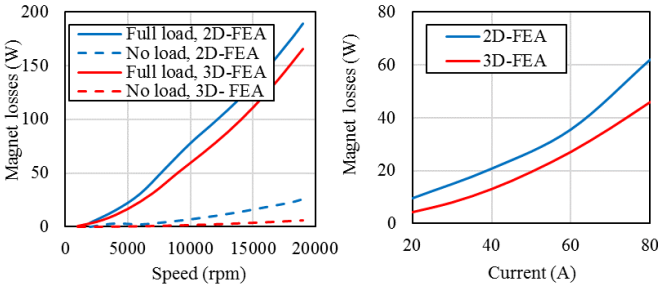

(a) Different speeds (b) Different q-axis currents

Fig. 7. Magnet losses at.

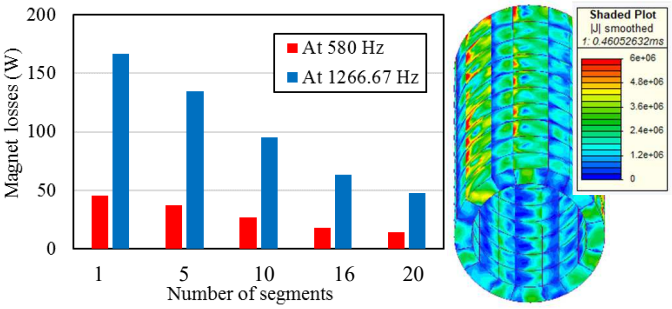

(a) Eddy current losses (b) Current density distribution

Fig. 8. Effect of PM segmentation on.

As a result, in order to achieve a balance between manufacturing costs and magnet losses, 10 segments of PM per pole were chosen, with magnet eddy current losses reduced by 43% at maximum speed. Indeed, as illustrated in Fig. 8 (b), having ten segments results in shorter pathways and hence reduced eddy current losses when compared to the non-segmented magnet shown in Fig. 6. (a).

D. *Windage Losses*

Windage losses in traditional machines are frequently smaller than electrical losses. On the other hand, windage losses can contribute considerably to total power losses and machine efficiency, in particular for high-speed machines with forced rotor cooling systems [17]. The coolant characteristics in such a cooling system are highly dependent on temperature, since the kinematic viscosity changes dramatically with temperature, potentially increasing drag torque at low temperatures [18]. Therefore, to have a better knowledge of windage losses and its effect on machine performance, it is very important to assess windage losses while taking into account different rotating speeds and temperatures. Windage losses were calculated analytically at different speeds up to 20 krpm in the temperature range of -40°C to +100°C, and obtained results are shown in Fig. 9. It can be observed that windage losses increase drastically at low operating temperatures, and as a result, the output torque required to accelerate the rotor decreases. Furthermore, the output torque should be around 0.3 Nm higher than the torque needed for driving the motor at the maximum speed and the maximum temperature and this value may rise to 3.5 Nm at the lowest operating temperature. Thus, it is desirable to raise the output torque of the electrical machine by a specific value in order to overcome the drag torque and deliver the required power.

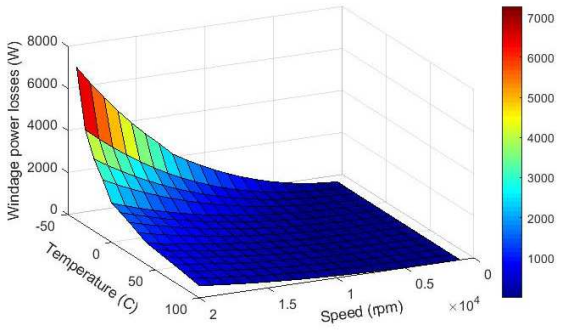

Fig. 9. Windage losses at various speeds and temperatures.

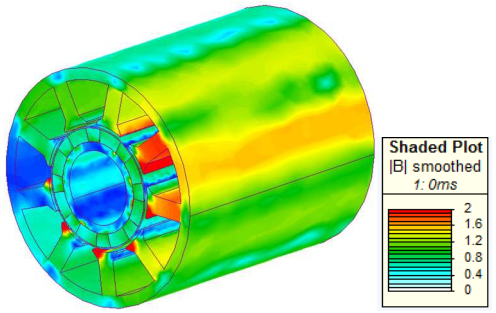

(a) 3D-map

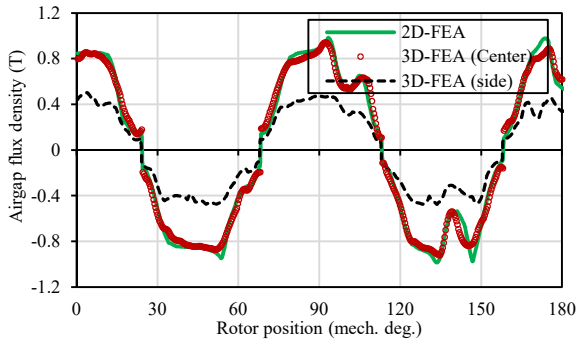

(b) Distribution

Fig. 10. No load flux density.

For the required application with coolant oil temperature equal to 90°C, windage losses account for 4% and 28% of total power losses at 8700 rpm and 19 krpm, respectively, while the drag torque ranges from 0 to 0.3 Nm across the speed range.

IV. Motor Performance

The performance of the designed motor is analyzed in this section at no-load and rated-load conditions. To achieve more accurate results, 3D FE simulations are performed, which account the impact of PM segmentation and end-effects.

A. Electromagnetic Analysis

The flux density map and the airgap flux density distribution are shown in Fig. 10 (a) and Fig. 10 (b) respectively. The 3D model shows the airgap flux density in two different zones: a) in the center of the axial length and b) at the rotor's end. As illustrated in Fig. 10 (b), the effect of end leakage results in a reduced amplitude and larger distortion of the airgap flux density at the machine's end. Axial leakage in 3D-FEA results in lower peak values than in 2D-FEA, despite the fact that the airgap flux density at the axial length's center is distributed similarly in both models.

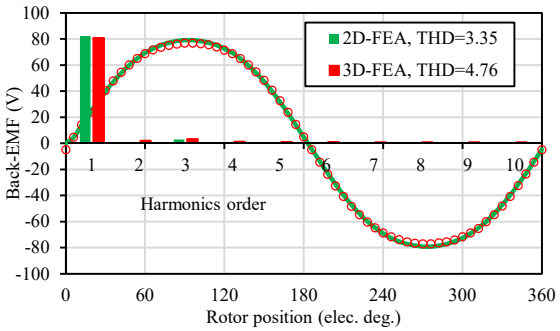

Fig. 11. The back-EMF waveform and its harmonics.

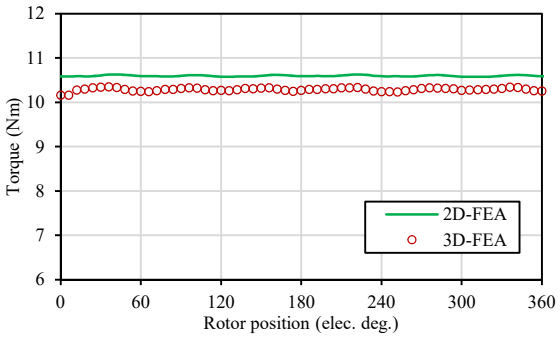

Fig. 12. Electromagnetic torque at full load condition.

Fig. 11 shows the no-load waveform of the PMSM's back-electromotive force (Back-EMF) and harmonics. At the rated speed of 8700 rpm, total harmonic distortion (THD) was 3.35% and 4.76% correspondingly for the result of 2D and the result of 3D FE. It is worth noting that when the end-windings are incorporated in the 3D model, the amplitude of the back-EMF decreases. This is because of the end-magnet leakage flux (3D-effect) that decreases the fundamental harmonic of the back EMF. The increase in the 3rd harmonic is mostly responsible for the increased THD.

To assess the electromagnetic torque and the torque ripple, the full load performance of the PMSM has been examined. The FEA-calculated machine torque waveform at full load condition with rated speed of 8700 rpm is shown in Fig. 12. The design provides significantly smooth torque due to low cogging torque and total harmonic distortion. For the 2D-FE model, the average torque is 10.5 Nm, with just 0.9% ripple. While these values are reduced to 10.3 Nm and 0.5% via a 3D-FE model. The K_T torque constant was also computed when just the machine's q-axis current was applied and the outcome of the 2D model was 0.1315 Nm⁄A, whereas the 3D model resulted in 0.1283 Nm/A.

In order to assess machine efficiency at different running speeds, previously estimated losses were utilized using FEA. Fig. 13, depicts the efficiency-speed characteristics of the PMSM. Low efficiency owing to significant copper losses was predicted in the low-speed area. Yet, the efficiency is enhanced at speeds of up to 11000 rpm and then subsequently reduces as speed rises further due to considerable losses in windage and rotor eddy current. Although the output power achieved by 3D-FEA modeling decreases, increased efficiency in high speed regions can be observed. This can be attributed to a reduction in rotor eddy current losses. In the final motor design, efficiency at speeds of 8700 and 19000 rpm, respectively, was 90.06% and 87.93% using 3D-FEA.

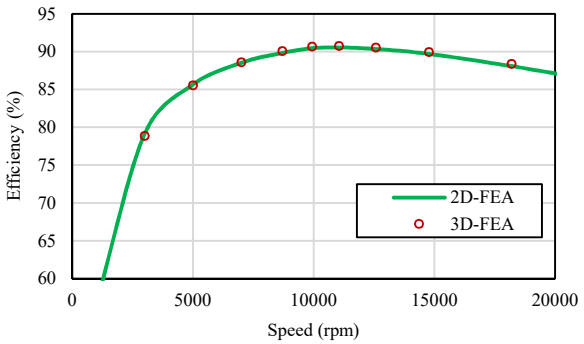

Fig. 13. Efficiency-speed characteristics.

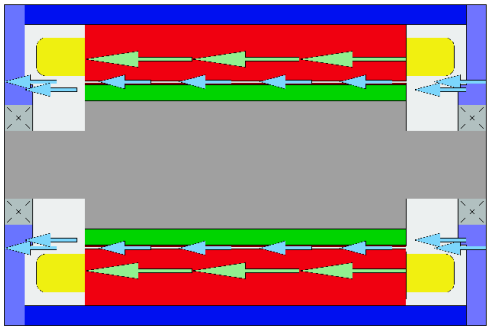

Fig. 14. Thermal model of PMSM in Motor-CAD.

TABLE II
THERMAL PROPERTIES OF THE MACHINE MATERIALS AND COOLING FLUID

Material	**Mass density (kg/m^3)**	**Specific heat capacity (J/kg/C)**	**Thermal conductivity (W/m/C)**
Stator steel (VacoFlux 48)	8120	460	30
Copper	8954	383.1	386
Wire insulation	1400	1000	0.2
Magnet (Sm_2Co_{17})	8300	350	10
Sleeve (Titanium)	4400	526	6.7
Shaft (17-4 PH Stainless steel)	7820	460	19.55
Air	1.2	103	0.026
Coolant oil (AEROSHELL FLUID 31)	851	2310	0.14
Housing (Aluminium)	2790	833	168

TABLE III
OPERATING TEMPERATURE OF DIFFERENT MACHINE PARTS

Machine Parts	**Temperature (°C)**
Windings	189.2
Stator core	141.8
PM	113.2
Sleeve	110
Shaft	112.7
Bearing	184.2

B. Thermal analysis

Thermal analysis considers power losses as heat sources. For the considered application, the highest losses are observed in the stator windings of the PMSM. Therefore, the total copper losses (i.e. AC+DC) must be included to ensure accurate estimation of temperature distribution.

(a) Rotor shaft without sleeve (b) Rotor shaft with sleeve

(c) Stator assembly (d) Final developed prototype

Fig. 15. 8p/9S PMSM.

The flooded cooling strategy permits direct contact between the cooling fluid and both the stator windings and the rotor, enhancing the heat dissipation. A cooling oil flow rate of 4 L/min with an oil inlet temperature of 90 °C, as defined by the project specifications was set. Indeed, under the worst-case scenario of a full-load condition at 19000 rpm, AC losses are expected to rise by 12% above DC values, resulting in total machine copper losses of 930W. Thermal analysis is carried out using Motor-CAD, and the thermal model is illustrated in Fig. 14. The heat transfer coefficients in electrical machine are derived from [19, 20]. Table II presents the thermal properties of machine materials, whereas Table III shows the temperature distribution within the machine. Despite the higher copper losses, the maximum temperature of the windings is 189°C, as shown in Table III. The increased copper losses do not result in serious issues with winding temperature since the proposed cooling system can keep the motor temperatures below the thermal limits of the materials, which for the case in hand is set as 210 °C corresponding to class C insulation. Meanwhile, the magnet temperature is less than 120°C, far below the magnet's limit temperature. As a result, the machine may be effectively cooled by the available oil flow.

V. EXPERIMENTAL TESTS

The proposed 8p/9s PMSM has been developed and experimentally validated. Fig. 15 (a and b) shows the rotor construction with segmented permanent magnets, quasi-Halbach array on the shaft without and with retaining sleeve, respectively. Whereas in Fig. 15 (c and d), the stator core with windings as well as the complete prototype are shown. In addition, the test platform, which comprises the components of the complete operating system used in the investigation, is illustrated in Fig. 16.

The no-load Back-EMF is one of the most significant motor characteristics since it influences machine performance. For the no-load test, the designed PMSM is driven by an IPM motor through a Magtrol torque-meter. A high bandwidth oscilloscope is also used to measure and record the back EMF.

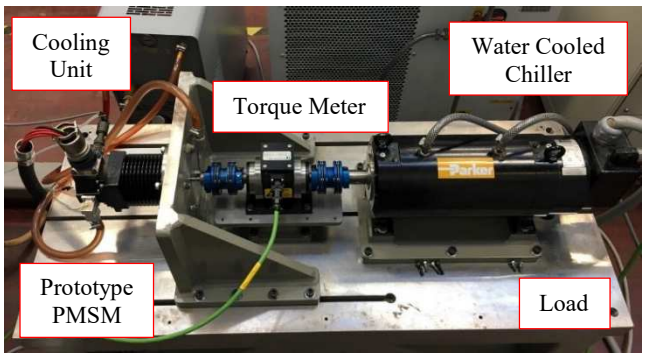

Fig. 16. Test-rig platform.

The experiments were conducted at different operating speeds, and the findings obtained are presented in Fig. 17. Clearly, the simulated and measured results are consistent with respect to the back-EMF. At no-load condition, the obtained back-EMF constant at maximum speed measures 0.0363 V·s/rad, which is only 5.46% lower than the one estimated using FEA. This is further corroborated by the measured waveform's harmonic content, which shows a THD of 0.6% at 19000 rpm.

The torque characteristics were measured at various phase current values ranging from 10 A to 80 A at a rated speed of 8700 rpm and an input DC voltage of 270 V as indicated in Fig. 18. On the basis of the experimental data, the computed torque constant with just q-axis current supplied to the machine (i.e. I_q=80 A, I_d=0 A) is 0.123 NmA, which is 6.9% less than that achieved using FEA simulations. The measured torque matches the predicted torque quite well. There is, however, a slight discrepancy as the current increases. This is mostly owing to the stator core's saturation effect that also increases leakage flux. In general, the developed motor shows close matching to the numerical models in predicting the electromagnetic performance of the motor.

VI. Conclusion

This paper provides an in-depth analysis of a high-performance PMSM designed for aerospace applications. The machine's performance at different operating conditions is examined by the 2-D and 3-D FE models, and the output findings are compared to experimental results to verify the electromagnetic design. The overall machine losses, including copper and core losses, as well as rotor eddy current and windage losses, are estimated and analyzed separately.

Also, the temperature distribution of the PMSM at the maximum running speed of 19000 rpm (the worst case scenario) is calculated on the basis of a lumped parameter network, and the reduction in the winding temperature rise may be achieved by a fully flooded cooling system. In particular, the aforementioned aspects should be more carefully considered for applications requiring higher performance and power density in order to provide an accurate evaluation of machine performance. This work demonstrated and proved the feasibility of the designed models for the high-performance machine, which were then validated experimentally.

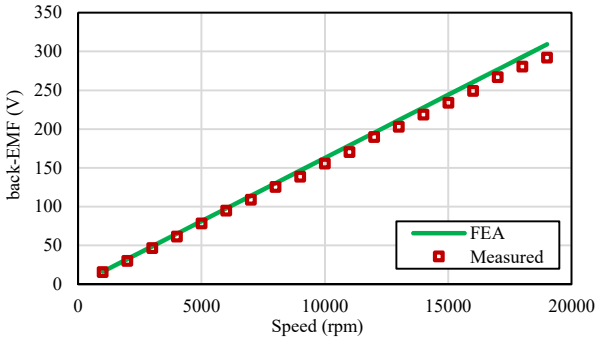

Fig. 17. Amplitude of the line-to-line back EMF as a function of speed.

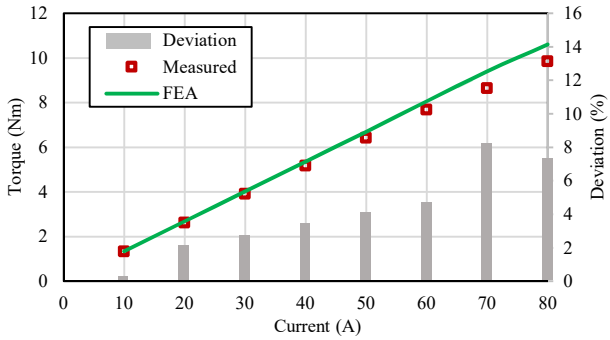

Fig. 18. Comparison between the measured and calculated torque vs Iq

VII. References

[1] P. Wheeler and S. Bozhko, "The More Electric Aircraft: Technology and challenges," in *IEEE Electrification Magazine*, vol. 2, n. 4, Dec. 2014.

[2] G. Qiao, G. Liu, Z. Shi, Y. Wang, S. Ma, and T.C. Lim, "A review of electromechanical actuators for More/All Electric aircraft systems," in *Proceedings of the Institution of Mechanical Engineers, Part C:Journal of Mechanical Engineering Science*, Nov. 2017.

[3] J. Fan, D. Ling, Z. Tang, and Z. Pei, "Study on nonlinear PID control for electro-hydrostatic actuator," in Guidance, Navigation and Control Conference (CGNCC), 2014 IEEE Chinese, 2014, pp. 1317-1320.

[4] N. Alle, S. S. Hiremath, S. Makaram, K. Subramaniam, and A. Talukdar, "Review on electro hydrostatic actuator for flight control," *International Journal of Fluid Power,* vol. 17, pp. 125-145, 2016.

[5] J. W. Bennett, B. C. Mecrow, A. G. Jack, and D. J. Atkinson, "A prototype electrical actuator for aircraft flaps," IEEE Transactions on Industry Applications, vol. 46, pp. 915-921, 2010.

[6] G. J. Atkinson, B. C. Mecrow, A. G. Jack, D. J. Atkinson, P. Sangha, and M. Benarous, "The Analysis of Losses in High-Power Fault-Tolerant Machines for Aerospace Applications," IEEE Transactions on Industry Applications, vol. 42, pp. 1162-1170, 2006.

[7] B. C. Mecrow, A. G. Jack, D. J. Atkinson, S. R. Green, G. J. Atkinson, A. King, et al., "Design and testing of a four-phase fault-tolerant permanent-magnet machine for an engine fuel pump," IEEE Transactions on Energy Conversion, vol. 19, pp. 671-678, 2004.

[8] G. Hong, T. Wei, X. Ding, and C. Duan, "Multi-Objective Optimal Design of Electro-Hydrostatic Actuator Driving Motors for Low Temperature Rise and High Power Weight Ratio," Energies, vol. 11, p. 1173, 2018.

[9] J. D. McFarland and T. M. Jahns, "Investigation of the Rotor Demagnetization Characteristics of Interior PM Synchronous Machines During Fault Conditions," in *IEEE Transactions on Industry Applications*, vol. 50, no. 4, pp. 2768-2775, July-Aug. 2014, doi: 10.1109/TIA.2013.2294997.

[10] N. Zhao, Z. Zhu, and W. Liu, "Rotor eddy current loss calculation and thermal analysis of permanent magnet motor and generator," *IEEE Transactions on Magnetics,* vol. 47, pp. 4199-4202, 2011.

[11] D. Zhang, F. Wang, and X. Kong, "Air friction loss calculation of high speed permanent magnet machines," in *Electrical Machines and Systems, 2008. ICEMS 2008. International Conference on*, 2008, pp. 320-323.
[12] M. Al-Ani *et al*., "Influence of Manufacturing and Drive Effects in High-Speed, High-Power-Density PM Machine for Flooded Pump Application," *2021 IEEE Workshop on Electrical Machines Design, Control and Diagnosis (WEMDCD)*, 2021, pp. 88-94.
[13] A. Al-Timimy et al., "Design and optimization of a high power density machine for flooded industrial pump," in Proc. XXII Int. Conf. Elect. Mach., Lausanne, Switzerland, 2016, pp. 1480–1486.
[14] A. Al-Timimy et al., "Trade-off analysis and design of a high power density PM machine for flooded industrial pump," in Proc. 42nd Ann. Conf. IEEE Ind. Electron. Soc., Florence, Italy, 2016, pp. 1749–1754.
[15] J. Shen, H. Hao, M. Jin and C. Yuan, "Reduction of Rotor Eddy Current Loss in High Speed PM Brushless Machines by Grooving Retaining Sleeve," in *IEEE Transactions on Magnetics*, vol. 49, no. 7, pp. 3973-3976, July 2013, doi: 10.1109/TMAG.2013.2243408.
[16] J. Gao, Y. Yu, and S. Huang, "Winding layers and slot/pole combination in fractional slot/pole PMSM—Effects on motor performance," in *2009 International Conference on Electrical Machines and Systems*, 2009, pp. 1-4.
[17] A. La Rocca, S. J. Pickering, C. Eastwick and C. Gerada, "Enhanced cooling for an electric starter-generator for aerospace application," *7th IET International Conference on Power Electronics, Machines and Drives (PEMD 2014)*, 2014, pp. 1-7, doi: 10.1049/cp.2014.0373.
[18] P. Ponomarev, M. Polikarpova, O. Heinikainen and J. Pyrhönen, "Design of integrated electro-hydraulic power unit for hybrid mobile working machines," *Proceedings of the 2011 14th European Conference on Power Electronics and Applications*, 2011, pp. 1-10.
[19] Y. Gai *et al*., "Cooling of Automotive Traction Motors: Schemes, Examples, and Computation Methods," in *IEEE Transactions on Industrial Electronics*, vol. 66, no. 3, pp. 1681-1692, March 2019.
[20] P. -O. Gronwald and T. A. Kern, "Traction Motor Cooling Systems: A Literature Review and Comparative Study," in *IEEE Transactions on Transportation Electrification*, vol. 7, no. 4, pp. 2892-2913, Dec. 2021.

VIII. BIOGRAPHIES

Ahmed Tameemi (M'18) received a Master's degree in electrical engineering from the University of Technology, Baghdad, Iraq, in 2012. He received the Ph.D. degree from the University of Nottingham, UK in 2019, with a focus on electromagnetic modeling and electrical machine design. Since 2019, he joined Al-Farahidi University, Iraq as an assistant professor. He has been working on several projects for the design of electrical machines for different applications. His main research interest includes the design and modeling of high-performance permanent magnet machines for industrial and aerospace applications.

Michele Degano (M'14 - SM'21) received the Master's degree in electrical engineering from the University of Trieste, Italy, in 2011, and the Ph.D. degree in industrial engineering from the University of Padova, Italy, in 2015. Between 2014 and 2016, he was a Postdoctoral Researcher at The University of Nottingham, U.K., where he joined the Power Electronics, Machines and Control (PEMC) Research Group. In 2016 he was appointed Assistant Professor in Advanced Electrical Machines, at The University of Nottingham, U.K. He was promoted Associate Professor in 2020. His main research focuses on electrical machines and drives for industrial, automotive, railway and aerospace applications, ranging from small to large power. He is currently the PEMC Director of Industrial Liaison leading research projects for the development of future hybrid electric aerospace platforms and electric transports.

Mauro Di Nardo received the M.Sc.(Hons.) degree in electrical engineering from the Polytechnic University of Bari (Italy) in 2012, and the Ph.D. degree in electrical machine design from the University of Nottingham (UK) in 2017. From 2017 to 2019 he was head of the AROL research team within the Polytechnic University of Bari leading industrial R&D projects on electrical drives design for mechatronics applications. Since the 2019, he joined the Power Electronics and Machine Control Group of the University of Nottingham as Research Fellow. His research interests are the analysis, modelling, and optimizations of electrical machines, including permanent magnet and synchronous reluctance topologies for automotive and aerospace sectors as well as induction motor for industrial applications.

Mukhammed Murataliyev (S'17-M'21) received his M.Sc. degree in electrical engineering from the University of Nottingham, Malaysia in 2016. He received a Ph.D. degree from University of Nottingham Ningbo China and UK in 2021, with a focus on novel synchronous reluctance motor design and optimization methods. Since 2021, he joined the Power Electronics and Machine Control Group of the University of Nottingham as a Research Fellow. His main research interest includes design and modeling of reluctance and permanent magnet machines for industrial and aerospace applications.

David Gerada (SM'21**)** received the Ph.D. degree in high-speed electrical machines from the University of Nottingham, Nottingham, U.K. in 2012. From 2007 to 2016, he was with the R&D Department, Cummins Inc. At Cummins, he pioneered the design and development of high speed electrical machines, transforming a challenging technology into a reliable one suitable for the transportation market, and establishing industry-wide used metrics for such machinery. In 2016, he joined the University of Nottingham as a Senior Fellow in Electrical Machines, responsible for developing state of the art electrical machines for future transportation, which push existing technology boundaries, while propelling the new technologies to high technology readiness levels. His research interests include novel materials and applications in electromechanical energy conversion, traction machines, mechatronics, etc. Dr. Gerada is currently a Chartered Engineer in the U.K. and a member of the Institution of Engineering and Technology.

Zeyuan Xu received the Ph.D. degree in mechanical engineering from The University of Manchester, Manchester, U.K., in 2002. He subsequently worked as a Research Fellow at the University Of Manchester Institute Of Science and Technology (UMIST), Manchester, Brunel University, Uxbridge, U.K., and the University of Nottingham, Nottingham, U.K. He is currently a Senior Research Fellow in thermomechanical design of high-speed electrical machines with the Power Electronics, Machines and Control Research Group, University of Nottingham. His main research interests include turbulent thermofluid flow, heat transfer enhancement, and thermal management of advanced electrical machines and power electronics.

Chris Gerada (SM'12) is an Associate Pro-Vice-Chancellor for Industrial Strategy and Impact and Professor of Electrical Machines. His principal research interest lies in electromagnetic energy conversion in electrical machines and drives, focusing mainly on transport electrification. He has secured over £20M of funding through major industrial, European and UK grants and authored more than 350 referred publications. He received the Ph.D. degree in numerical modelling of electrical machines from The University of Nottingham, Nottingham, U.K., in 2005. He subsequently worked as a Researcher with The University of Nottingham on high-performance electrical drives and on the design and modelling of electromagnetic actuators for aerospace applications. In 2008, he was appointed as a Lecturer in electrical machines; in 2011, as an Associate Professor; and in 2013, as a Professor at The University of Nottingham. He was awarded a Research Chair from the Royal Academy of Engineering in 2013. Prof. Gerada served as an Associate Editor for the IEEE Transactions on Industry Applications and is the past Chair of the IEEE IES Electrical Machines Committee.